JOURNAL OF THE ROYAL SOCIETY Interface

Determination and validation of the elastic moduli of small and complex biological samples: bone and keratin in bird beaks

Joris Soons, Anthony Herrel, Peter Aerts and Joris Dirckx

J. R. Soc. Interface 2012 **9**, 1381-1388 first published online 16 November 2011
doi: 10.1098/rsif.2011.0667

JOURNAL OF THE ROYAL SOCIETY Interface

J. R. Soc. Interface (2012) **9**, 1381–1388
doi:10.1098/rsif.2011.0667
Published online 16 November 2011

Determination and validation of the elastic moduli of small and complex biological samples: bone and keratin in bird beaks

Joris Soons[1,*], Anthony Herrel[2,3], Peter Aerts[3,4] and Joris Dirckx[1]

[1]*Laboratory of Biomedical Physics, University of Antwerp, Groenenborgerlaan 171, B2020 Antwerpen, Belgium*
[2]*Département d'Ecologie et de Gestion de la Biodiversité, Museum National d'Histoire Naturelle, 57 rue Cuvier, Case postale 55, 75231 Paris Cedex 5, France*
[3]*Department of Biology, University of Antwerp, Universiteitsplein 1, B2610 Antwerpen, Belgium*
[4]*Department of Movement and Sports Sciences, University of Ghent, Watersportlaan 2, B9000 Ghent, Belgium*

In recent years, there has been a surge in the development of finite-element (FE) models aimed at testing biological hypotheses. For example, recent modelling efforts suggested that the beak in Darwin's finches probably evolved in response to fracture avoidance. However, knowledge of the material properties of the structures involved is crucial for any model. For many biological structures, these data are not available and may be difficult to obtain experimentally given the complex nature of biological structures. Beaks are interesting as they appear to be highly optimized in some cases. In order to understand the biomechanics of this small and complex structure, we have been developing FE models that take into account the bilayered structure of the beak consisting of bone and keratin. Here, we present the results of efforts related to the determination and validation of the elastic modulus of bone and keratin in bird beaks. The elastic moduli of fresh and dried samples were obtained using a novel double-indentation technique and through an inverse analysis. A bending experiment is used for the inverse analysis and the validation of the measurements. The out-of-plane displacements during loading are measured using digital speckle pattern interferometry.

Keywords: finite-element modelling; biomechanics; inverse analysis; double indentation; digital speckle pattern interferometry

1. INTRODUCTION

In recent years, there has been a surge in the development of finite-element (FE) models aimed at testing hypotheses concerning the design of biological structures (see reviews in [1–4]). However, in any FE model, it is crucial to incorporate the material properties of the tissues included in the model [3,5,6]. Yet, for many biological structures, these data are not available in the literature and may be difficult to obtain given the complex nature of biological materials. Moreover, biological structures are often composed of multiple layers that may vary in their mechanical properties, further enhancing the complexity of the models and the need for accurate input data. Indeed, the mechanical interaction between multiple layers will change drastically depending on the material properties used. The beaks of birds, turtles and probably some dinosaurs as well are good examples of such complex multi-layered biological structures consisting of a horny external layer with underlying bone and a (epi-)dermal layer in between [7]. Bird beaks are particularly interesting structures as they appear to be highly optimized in some cases. Indeed, in birds that use their beaks to crack hard seeds, the beak has to be heavily built and strong enough to withstand failure during biting, but still light enough to allow efficient flight [8,9]. Consequently, natural selection on the beak in seed-cracking birds is thought to push towards an optimum with a maximal strength yet minimal amount of material within the limits imposed by trade-offs and biological constraints. Recent modelling efforts suggested that the beak in Darwin's finches evolved in response to fracture avoidance [9], thus explaining selection on beak dimensions observed in natural populations [10]. However, these models need to be refined further. Indeed, only the geometry of the bony upper beak, without the keratin layer, was considered and, in addition, no material properties specific to these bird beaks were included.

Given the complexities involved with obtaining fresh material of highly protected species such as Darwin's finches, we used the Java finch (*Padda oryzivora*) to

*Author for correspondence (joris.soons@ua.ac.be).

Received 30 September 2011
Accepted 24 October 2011

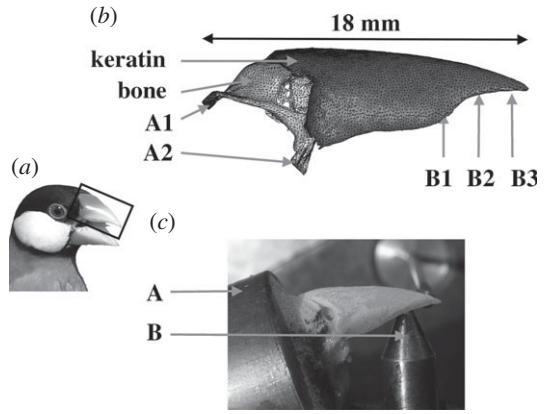

Figure 1. (*a*) Head of the Java finch (*Padda oryzivora*) in which the upper beak is indicated. (*b*) FE model of the upper beak with keratin and bone indicated (see §2.3). (*c*) Experimental set-up for the bending experiment (see §2.2 and figure 2). 'A' denotes the sample holder filled with polyester resin to constrain the bending area (A1) and jaw bones (A2). 'B' denotes the seed reaction force imitated by an indentation at three different positions: at the centre of the upper beak (B1), at the tip near the limit of the bony core (B2) and at the rostral-most aspect of the keratinous upper beak (B3).

investigate the material properties of the tissues of the upper beak in order to build realistic FE models. Java finches are typical seed-cracking birds that use their beaks to manipulate and crack seeds [11]. The upper beak in this species (figure 1) is 1–2 cm long and the keratin layer is a few 100 μm thick [7]. A large range of possible moduli can be found in the literature, with values for keratin varying from 1 to 7 GPa and those for bone varying from 7 to 30 GPa for compact bone and down to 0.01 GPa for cancellous bone [12]. Furthermore, the elastic modulus of keratin seems to depend on its humidity [13]. Given the wide range of bone moduli reported in the literature, the Young modulus needs to be determined experimentally for the tissues of interest. However, acquiring this modulus on biological samples is not straightforward. Tensile tests are difficult to perform as obtaining samples with a well-defined geometry is challenging. Here, we propose two techniques to quantify the Young moduli in bone and keratin of the beak of the Java finch. First, a double-indentation technique designed to measure thin biological samples [14,15] is used. Second, an inverse analysis is performed: in an FE model, we adjust the material properties to obtain the best fit between a model and an experimental measurement quantifying actual beak deformation using digital speckle pattern interferometry (DSPI). DSPI has been used as a validation tool in some previous biological FE analyses [16–21], because it has some important advantages over standard measurement techniques, such as strain gauges: displacements can be acquired with high accuracy and full field and are contactless.

2. MATERIAL AND METHODS

2.1. Double-indentation technique

Standard tests to measure the Young modulus exist, but they have some drawbacks when used on small and thin samples, such as the pieces which can be harvested from

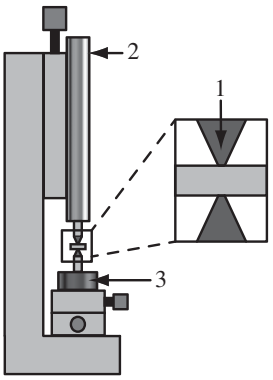

Figure 2. Experimental set-up of the double-indentation technique. (1) Two needles with the clamped sample, (2) the piezo-actuator to introduce displacement, and (3) a load cell to measure the reaction force.

the Java finch's upper beak. Standard tensile tests need samples of a specific geometry and well-controlled boundary conditions. These requirements are very hard to meet on samples of a few millimetres and only a few hundreds of micrometres thick. An alternative approach is the use of micro- or nano-indentations. If the reaction force of a certain indentation is obtained, one can calculate the modulus using Sneddon's solution [22]. Nevertheless, this theorem is valid only for samples that are relatively thick when compared with the indenting needle. Reducing the needle radius enables measurements on thinner samples. However, anomalies can be expected for biological tissues since the mechanical response of the microstructures will be measured instead of the bulk properties, which is what is needed for FE modelling.

Recently, we developed a method to measure the bulk modulus of thin samples. First, we expanded Sneddon's solution to thin samples by adding a correction factor. Next, we added a second needle (figure 2) to avoid problems at the contact zone between the randomly shaped sample and the sample stage. Indeed, the introduced stress will only have a local effect if the needle is negligibly small. If, however, a thin sample is placed on a flat bed and is indented only by one needle, a slightly bent sample may also bend depending on the way it makes contact with the flat bed. Therefore, we used needles placed symmetrically at both sides of the sample. Consequently, the material is clamped between the two needles and hence a virtual mirror plane is introduced. This mirror plane will have the same behaviour as a perfect sliding interface on a flat sample stage, allowing the needle-radius to be increased for thin samples and thus avoiding microstructural effects. In practice, an indentation of 1 μm is performed using a piezo-actuator (PI P-841.60) and the reaction force is measured with a load cell (Sensotec model 31; 50 N range). The indentation point can be positioned precisely with micrometre screws. Polishing of the samples can be necessary since the non-flatness of the sample should be smaller than the offset indentation depths, approximately between 5 and 10 μm. More information about the double-indentation technique can be found in a previous paper dealing with the elastic modulus of middle ear ossicles [15].

We used the double-indentation technique to obtain the Young modulus of the keratin layer and the bony

core of the Java finch's upper beak. In total, seven Java finches were examined. The first group of four finches was selected (*Padda* 1, 2, 3 and 4) for dry testing. After sacrificing the birds with CO_2 gas, bone and keratin of the upper beak were carefully dissected using a scalpel, resulting in square samples of a few millimetres wide and with a thickness ranging between 50 and 500 μm. Taking samples from the corner of the upper beak was avoided since they have too large a curvature. Keratin on top and at the bottom of the upper beak was harvested separately for *Padda* 2, 3 and 4.

The samples were polished to obtain flatter surfaces for the indentation. Indentation tests were performed 2 h post-mortem, yielding the elastic modulus for dried samples. We expected a large variation for keratin depending on its humidity [13]. Therefore, the modulus of the keratin of a group of three Java finches (*Padda* 5, 6 and 7) was measured during dehydration. The following exponential fit was used to model the evolution of the modulus as a function of time during the process of dehydration:

$$E(t) = (E_{\text{fresh}} - E_{\text{dry}})\left(1 - \exp\left(\frac{-t}{\tau}\right)\right) + E_{\text{dry}}. \quad (2.1)$$

$E(t)$ is the measured modulus during drying out at time t, E_{fresh} is the modulus for fresh samples ($t = 0$), E_{dry} is the modulus for dried samples ($t = \infty$) and τ is the time constant. The Matlab curve fitting toolbox was used to calculate the best fit to the measured moduli. Keratin of *Padda* 5 was tested directly after harvesting. Bone and keratin samples of *Padda* 6 and 7 were studied moist before carrying out the actual exponential-fit measurements. An ultrasonic humidifier was used to keep them moist during dissection and testing.

All the samples were several millimetres in length and width and had a thickness of a few hundred micrometres. The exact thickness was measured to calculate the FE correction factor for Sneddon's equation. The indentation was performed at different positions and different depths (approx. from 5 to 10 μm).

2.2. Digital speckle pattern interferometry bending experiment

We constrained the jaw bone and applied a force using a stepper motor-driven non-rotating spindle that ends in a cone (steps of 16 nm per motor step; PI M-235.2DG). The flattened and polished point of the cone puts a displacement of a few micrometres at the bottom of the upper beak. The polished indentation point can be positioned precisely with micrometre screws allowing controlled and repeated loading of the upper beak. Three different positions were selected (indicated in figure 1) at the centre of the upper beak, at the tip near the limit of the bony core and at the rostral-most aspect of the keratinous upper beak. The indentation was chosen such that it was approximately perpendicular to the indented surface. A photograph was taken to retrieve the boundary conditions for the FE model. The reaction force was measured with a load cell (Sensotec 31, 5 N range) attached at the indentation point. The back of the skull and the jaw bones were constrained in a sample holder filled with polyester resin (VIAPAL 223BS/65).

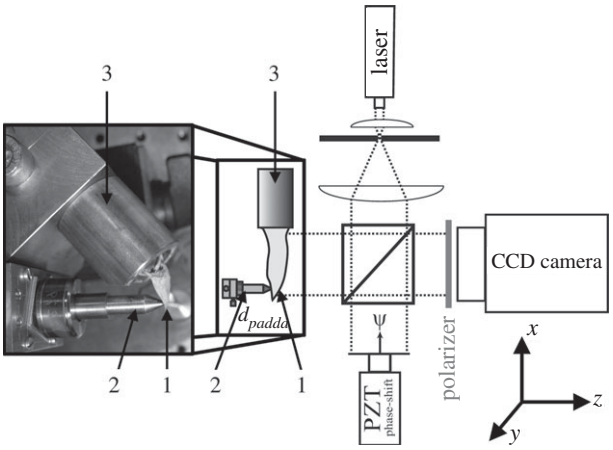

Figure 3. Bending experiment and DSPI set-up: (1) the upper beak, (2) the polished indentation point mounted on a load cell, and (3) the sample holder filled with polyester resin. CCD, charge-coupled device.

A group of three further Java finches (*Padda* 8, 9 and 10) was prepared without special precautions to prevent dehydration. After sacrificing the animals, the head was harvested and the skull was cleaned, removing most of the non-bony parts such as feathers, eyes, muscles and brain tissue. The back of the skull was dried with ethanol to obtain a good bonding with the casting resin that was used to fixate the skull in a specimen holder. Next, the lower beak was removed, allowing us to position the polished point and imitate the seed reaction force. Finally, the skull was placed in a sample holder which was then filled with polyester resin. A curing time of 2 days between placing the samples in the holder and carrying out the actual experiments is necessary. A magnesium oxide coating was used to improve the light reflectance.

The out-of-plane displacement on the topside of the upper beak, introduced by the bending experiment, was quantified using a DSPI set-up (figure 3). A He–Ne laser beam ($\lambda = 632.8$ nm) was expanded using a beam expander and a beam splitter was used to illuminate the top of the upper beak and a reference plane. Owing to the optical roughness of the surfaces, a speckle pattern is generated on both the beak and the reference plane. Both speckle patterns were combined with the beam splitter, and the interference pattern was recorded with a charge-coupled device camera (AVT Pike F-505, 16 bit, 2 charge-coupled device kpx [2], with a telecentric lens). Pearson's correlation was used between the interference pattern of the non-deformed and the deformed state. As such, the out-of-plane displacement was obtained. Indeed, an out-of-plane deformation of $\lambda/4$ changes constructive interference into destructive interference, thus resulting in no correlation. An interval of 5 s between imaging of the non-deformed and deformed beaks was introduced to minimize visco-elastic effects. Using highly accurate translation of the reference plane, four phase-shifted speckle patterns were obtained for the beak in the resting position. Using these images and the speckle patterns of the beak in the deformed position, full-field out-of-plane beak displacement could be calculated with sub-wavelength resolution. The entire set-up was placed on an optical table to reduce vibration errors [16].

We decided to use the derivative of this displacement along the x-direction as it is a more important parameter for the bending than the z-displacement (out-of-plane) itself, as any rigid body movement yields only a constant for the derivative [23]. The signal-to-noise ratio was improved by conducting multiple measurements (20–100 for one experiment). These measurements were combined by dividing the actual displacement with the measured force. Using a moving average smoothing with a window size of 5×5 prevented errors in the derivative. The results of this bending experiment were used as a validation experiment for the FE model and in the inverse analysis (§2.4).

2.3. Finite-element model

In order to conduct an inverse analysis, an FE model of the bending experiment (described in §2.2) was used. The construction and validation of the FE model and the results of realistic loading experiments will be described in detail in a forthcoming paper. In brief, one *Padda* was scanned at the European Synchrotron Radiation Facility (ESRF, Grenoble, France). Images of (2 kpx) [2] with a resolution of 45 µm were obtained. Keratin and bone were segmented semi-automatically based on greyscale thresholding using Amira 4.1 (64-bit version, TGS Systems). A Delaunay tetrahedralization was conducted using the TetGen software package [24]. A tetrahedral grid with approximately 700 k linear elements was generated after convergence testing on the out-of-plane displacement results (<5%).

The mesh was imported in the FE program FEBio [25]. The fixation of the polyester resin was imitated by a translational and rotational constraining of the elements at the bending area and the upper jaw (A1 and A2 in figure 1). A 1 N indentation force was introduced at the corresponding elements. Finally, we scaled the upper beaks to the same dimension as used in the experiments (*Padda* 8–13). Photographs of the experimental set-up were used for the scaling and estimation of the boundary conditions. The Poisson ratio for bone and keratin is 0.4 [26,27] and the Young moduli were changed in the inverse analysis as described below.

2.4. Inverse analysis

Inverse modelling is a technique where parameters of a model are explored by maximizing the fit between experimental and model data. Here, the best fit to the derivative of the z-displacement (out-of-plane) along the x-direction was determined. The major advantage of an inverse analysis is the *in situ* parameter determination. We used the measurement results of the bending experiment described in §2.2 and adapted the parameters in the corresponding FE model described in §2.3. The goodness-of-fit is described with a coefficient of determination R^2,

$$R^2 = 1 - \frac{\mathrm{SS_{err}}}{\mathrm{SS_{tot}}},$$

$$\mathrm{SS_{err}} = \sum_{i=1}^{N} (\mathrm{Exp}(q_i) - \mathrm{FE}(q_i))^2,$$

$$\mathrm{SS_{tot}} = \sum_{i=1}^{N} (\mathrm{Exp}(q_i) - \overline{\mathrm{Exp}})^2$$

and

$$\overline{\mathrm{Exp}} = \frac{1}{N} \sum_{i=0}^{N} \mathrm{Exp}(q_i).$$

$\mathrm{Exp}(q_i)$ represents the values of the derivative of the out-of-plane displacement along the x-direction for point q_i, obtained in the DSPI experiment, and $\mathrm{FE}(q_i)$ represents the values for this derivative in the FE model. Since DSPI is a full-field method, we calculated R^2 for all N points on the upper beak surface, except for the noisiest parts and the bending area itself. Rigid body movements, which are not interesting from a mechanical point of view, are removed by subtracting the mean values and thus centring the results around zero. The closer the R^2 values are to the value of 1, the better the fit. Our final R^2 value was a combination of the results for the loading scenarios at the three different positions.

Changing the Young modulus of bone and keratin in the FE model will result in a different R^2 value. Our goal was to obtain the highest R^2 value, because it indicates the best fit between the experiment and the FE model. The maximum in a selected domain of moduli can be obtained with surrogate modelling. In such a surrogate model, every Young's modulus for keratin and bone is linked to a corresponding R^2 value (see below). The Matlab SUMO toolbox was used to create a good surrogate model with a low calculation cost [28]. Finally, we selected the highest R^2 in the surrogate model.

3. RESULTS

3.1. Double-indentation technique

Bone samples were between 50 and 130 µm thick, the keratin on the dorsal side of the upper beak was between 40 and 200 µm thick, and the tested keratin on the ventral side of the upper beak had a thickness of between 250 and 500 µm. One indentation cycle, including preconditioning and measurement on three depths (5–10 µm), took approximately 1 min. The mean values and standard deviations for the elastic modulus of bone and keratin of the dried upper beak (*Padda* 1, 2, 3 and 4) are shown in table 1. For *Padda* 2, 3 and 4, we obtained the modulus of the keratin on top and at the bottom of the upper beak separately.

The obtained moduli for bone and keratin of moist samples and their standard deviations are presented in table 2. Figure 4 shows the data for the Young modulus and the exponential fit for the keratin of *Padda* 5 during drying. For the three finches an average value of 35 min with a standard deviation of 21 min was obtained for the time constant of the exponential, which describes the change of the modulus as a function of time during dehydration (equation (2.1)). The average time constant for keratin coming from the bottom of the beak was 38 min and from the top was 32 min. The asymptotic values (E_{dry}), which are the moduli of

Table 1. Mean values and standard deviations for the Young modulus measured with the double-indentation technique on dry samples. The first four Java finches were tested when dried out, the following three were tested during drying out and the exponential fit of equation (2.1) was used to obtain E_{dry}. The results for the modulus of bone (E_{bone}), keratin ($E_{keratin}$), keratin on top of the upper beak (E_{topker}) and at the bottom ($E_{bottomker}$) are presented.

	E_{bone} (GPa)	$E_{keratin}$ (GPa)	E_{topker} (GPa)	$E_{bottomker}$ (GPa)
Padda 1	7.3 ± 2.0	2.85 ± 0.69		
Padda 2	7.5 ± 2.5	2.87 ± 0.85	2.88 ± 0.85	2.86 ± 0.87
Padda 3	8.4 ± 3.9	3.06 ± 0.69	3.06 ± 0.64	3.06 ± 0.65
Padda 4	7.8 ± 3.4	2.55 ± 0.75	2.43 ± 0.75	2.58 ± 0.68
Padda 5 (exponential fit)		3.31 ± 0.69	3.59 ± 0.51	2.90 ± 0.83
Padda 6 (exponential fit)	7.7 ± 3.0	3.37 ± 0.69	3.66 ± 0.74	3.12 ± 0.57
Padda 7 (exponential fit)	6.5 ± 3.5	3.34 ± 0.80	3.39 ± 0.85	3.22 ± 0.74
weighted average	7.5 ± 1.2	3.1 ± 0.3	3.2 ± 0.3	3.0 ± 0.3

Table 2. Elastic modulus of bone (E_{bone}), keratin ($E_{keratin}$), keratin on top of the upper beak (E_{topker}) and at the bottom ($E_{bottomker}$) for fresh samples, measured by keeping the samples moist during and after harvesting.

	E_{bone} (GPa)	$E_{keratin}$ (GPa)	E_{topker} (GPa)	$E_{bottomker}$ (GPa)
Padda 6	7.6 ± 3.5	1.59 ± 0.47	1.45 ± 0.46	1.74 ± 0.43
Padda 7	6.6 ± 3.0	1.78 ± 0.68	1.90 ± 0.74	1.62 ± 0.55
weighted average	7 ± 2	1.7 ± 0.4	1.6 ± 0.4	1.7 ± 0.3

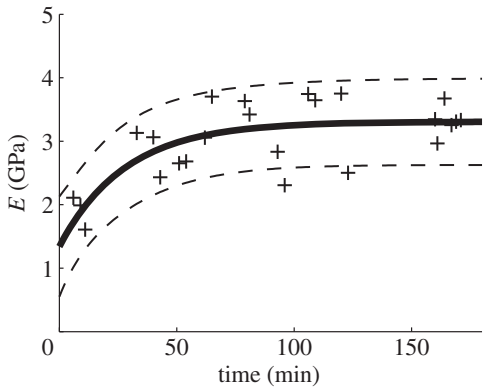

Figure 4. Elastic modulus of keratin from *Padda* 5 during drying out. The crosses indicate the average of three measurements on different depths (5–10 μm); the solid line is the exponential fit; and the dashed lines indicate the 68% confidence bounds.

the dried samples, and the 68 per cent confidence limits, are presented in table 1. It should be noted that the values of *Padda* 5 were measured directly after harvesting; *Padda* 6 and 7 were kept moist for a period of approximately 2 h. The exponential fit also yields the values for the fresh samples (E_{fresh}). These values are presented in table 3. We took approximately 15 indentation cycles to calculate the presented averages and exponential fits and we removed the outliers.

3.2. Inverse analysis

The derivative of the out-of-plane displacement along the x-direction for tip-loading of *Padda* 8 is presented in figure 5. In figure 5*a*, the results measured with the DSPI set-up are illustrated, while in figure 5*b* the same results can be seen for a FE model. This model was optimized through an inverse analysis. The cross-sectional results can be seen in figure 6. Figure 7 shows a surrogate model of *Padda* 8, linking the elastic modulus of bone and keratin to a corresponding R^2 for the three bending experiments combined. The maximum of this surrogate model indicates that the optimal modulus is 8.0 GPa for bone and 2.8 GPa for keratin (table 4).

Table 3. Elastic modulus of keratin ($E_{keratin}$), keratin on top of the upper beak (E_{topker}) and at the bottom ($E_{bottomker}$) for fresh samples, calculated with the exponential fit from equation (2.1).

	$E_{keratin}$ (GPa)	E_{topker} (GPa)	$E_{bottomker}$ (GPa)
Padda 5	1.34 ± 0.79	1.87 ± 0.56	0.7 ± 2.2
Padda 6	1.72 ± 0.72	1.40 ± 0.66	2.14 ± 0.78
Padda 7	1.76 ± 0.80	1.73 ± 0.88	1.72 ± 0.75
weighted average	1.6 ± 0.4	1.7 ± 0.4	1.8 ± 0.5

4. DISCUSSION

4.1. Dry samples

The results of the elastic modulus obtained with the double-indentation experiment are presented in table 1. A weighted average for the modulus of all seven examined Java finches (*Padda* 1–7) of 7.5 GPa for bone and 3.1 GPa for keratin was obtained. There is a small difference between the two sets of measurements. We obtained a weighted average for the modulus of keratin of 2.8 ± 0.4 GPa for *Padda* 1–4 and of 3.3 ± 0.4 GPa for *Padda* 5–7. The small difference may be caused by the fact that the measurements were not performed on entirely dry samples for *Padda* 1–4. The relative error for the acquired moduli is however less than 16 per cent. This

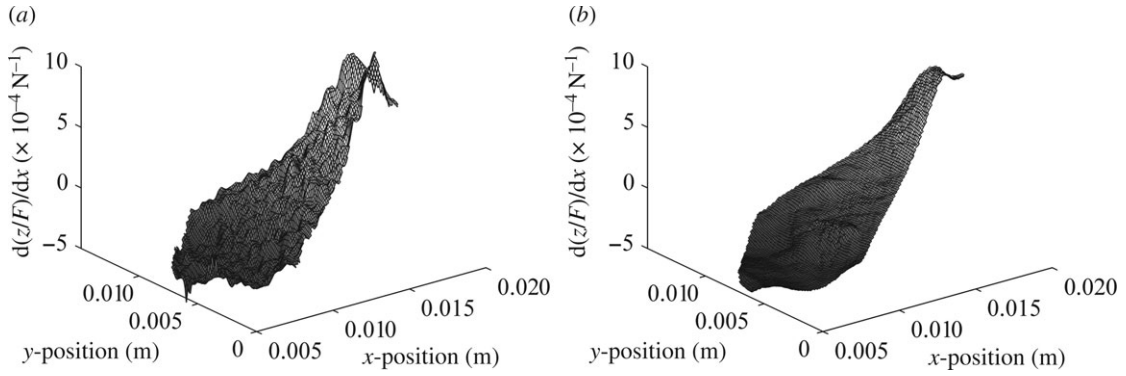

Figure 5. Full-field upper beak results for a tip-loading bending experiment of *Padda* 8 (dry): the derivatives of the out-of-plane displacement along the x-direction are shown for (a) the DSPI experiment and (b) the FE model.

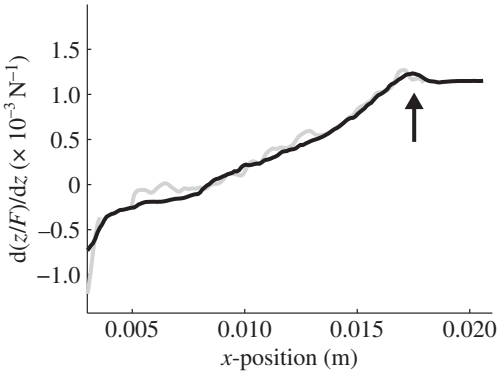

Figure 6. Cross-sectional result ($y = 6$ mm; see figure 5) for tip loading of *Padda* 8 (dry): the derivatives of the out-of-plane displacement along the x-direction are shown for the DSPI experiment (grey line) and the FE model (black line). The arrow indicates the indentation point.

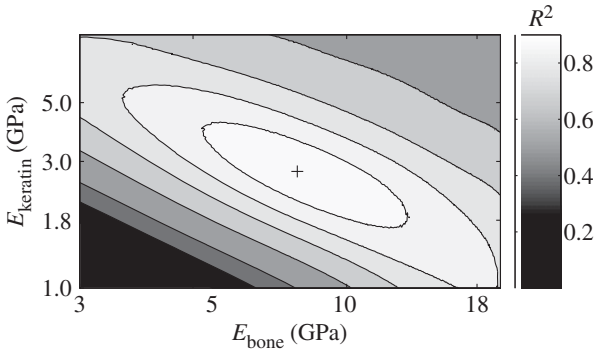

Figure 7. Surrogate model of *Padda* 8 (dry), which links the modulus of keratin and bone in the FE model to a corresponding R^2 (for the bending experiments: tip, centre and total tip loading). The optimal modulus of 8.0 GPa for bone and 2.8 GPa for keratin ($R^2 = 0.90$) is indicated with a cross. Notice the logarithmic scale.

precision is high for biological tissues, which are subject to inter- and intra-specimen variability, and suggests that our method provides consistent results. Moreover, the high precision of the keratin modulus suggests no significant difference in values for keratin on the top and at the bottom of the upper beak.

The DSPI results for the bending experiment show a rather smooth derivative (figure 6), indicating low noise in the original displacement measurement. In addition, good results were obtained with the inverse analyses based on the DSPI experiment (table 4). Indeed, all R^2 values are above 0.90, suggesting a very good fit of the model to the experimental data. Those findings also demonstrate that DSPI is an appropriate tool for FE model validation. It yields some major benefits when compared with other techniques, such as strain gauges, which are commonly used in biomechanical research. DSPI delivers full-field measurements and, as it is an optical technique, the experiments can be done without disturbing the sample. Non-contact measurements are important for measurements on softer tissue. Finally, the out-of-plane displacement can be obtained with a very high precision (submicron resolution). A major drawback of DSPI is the high requirements for stability, making it impossible to perform measurements *in vivo*.

The surrogate model (figure 7) returns an R^2 value for every elastic modulus of bone and keratin in the selected domain. Very high R^2 values are obtained, suggesting a high correlation between the model and the DSPI measurements. It should be noted that we ignored the noisiest parts, resulting in slightly higher R^2 values. We also ignore the bending at the back of the beak, which shows a divergence between the results obtained through DSPI and the FE model. The discrepancy at the bending area could be caused by model constraint errors in this region. More specifically, we think that it can also be caused by lower bone density and a supporting bony layer, which are not present in our FE model.

The lower bone density will result in a lower elastic modulus and will thus introduce an extra rigid body movement. This rigid body movement will result in an extra constant for the derivative, which is ignored by averaging both results around zero.

Our inverse analysis allows us to obtain optimal Young's moduli. Interestingly, the surrogate model displays a ridge of high R^2 values. Indeed, less stiff bone can be compensated by stiffer keratin and vice versa. More noise in the experiment will result in a poorer selection of the optima and thus only a limited set of moduli can be selected on the ridge (§4.2). The results presented in table 4 were obtained through a combined

Table 4. Elastic moduli of bone (E_{bone}) and keratin ($E_{keratin}$) for three Java finches (*Padda* 8, 9 and 10) using samples that were dried before testing. The values were obtained through an inverse analysis (corresponding R^2 values are given) for three bending experiments (centre, tip and total tip loading).

at three positions	E_{bone} (GPa)	$E_{keratin}$ (GPa)	R^2
Padda 8	8.0	2.8	0.90
Padda 9	7.0	3.6	0.94
Padda 10	6.7	3.1	0.93
average ($n = 3$)	7.2 ± 0.7	3.1 ± 0.4	

optimization: one optimum is obtained by combining the results of three different bending experiments, which should provide more stable results since experiments with a smaller R^2 contribute less to the combined R^2. In addition, a specific selectivity for some experiments is expected. For instance, a tip loading at a location where there is no bony core will result in a better selectivity for keratin.

A weighted averaging for the elastic moduli of the three tested finches (*Padda* 8–10) resulted in an elastic modulus of 7.2 GPa for bone and 3.1 GPa for keratin, both with a relative error smaller than 13 per cent. This small value suggests a rather high precision of this technique. In addition, as both the double-indentation technique and the inverse analysis yield similar values, this suggests that both techniques provide reliable and accurate results. Combining results from both approaches provides a weighted average of 7.3 ± 0.6 GPa for the modulus of bone and 3.1 ± 0.2 GPa for keratin. The obtained values lie within the range $1\ \text{GPa} < E_{keratin} < 7\ \text{GPa}$ and $7\ \text{GPa} < E_{bone} < 30\ \text{GPa}$, given by Meyers *et al.* [12]. Compared with other literature values of bone [29], the modulus we found is rather low. Literature values for keratin correspond well with our results [13]. The wide variety of bone and keratin samples in the literature indicates the importance of measurements on the actual samples to be modelled.

4.2. Fresh samples

The consistency between the results for dry samples obtained using the double-indentation technique and inverse analysis indicates the reliability of both the techniques. We may therefore expect that the double-indentation technique will also function well for measurements on fresh samples. Consequently, this technique will enable us to obtain a good estimation of the linear elastic moduli for *in vivo* bone and keratin. These material parameters will be of high importance to build a realistic FE model.

Two strategies were used for the double-indentation technique to obtain the elasticity modulus of fresh samples. The first strategy was to keep the samples moist during harvesting and double-indentation testing. In practice, this also enables the testing of bone samples that need a longer preparation time. Moreover, more tests can be performed, resulting in a better error analysis. The weighted averages for *Padda* 6 and 7 are given in table 2. The second strategy used the exponential fit from equation (2.1) and the moduli obtained during drying, resulting in a modulus before and after drying out. A time constant (τ) of 35 ± 21 min was observed for the dehydration process of keratin. The dehydration of keratin obtained from the top of the beak has a slightly lower time constant of 32 ± 17 min, which can be explained by its thinness. The large variability in the measurements of the time constants can be explained by the impossibility of controlling air humidity and consequently the desiccation rate.

The time constant is clearly higher than the measurement time of 1 min, which allowed us to use the exponential fit for our data. No significant difference was found between a sample measurement directly after harvesting (*Padda* 5) and the measurement of samples which were kept moist (*Padda* 6, 7). No exponential fitting was done for bone, as there was no significant difference between the moist and dry elastic modulus. The weighted average for the Young modulus of moist bone is 7 ± 2 GPa. The weighted average for the modulus of moist keratin, obtained by the double-indentation technique, is 1.7 ± 0.4 GPa. No significant difference for keratin taken from the bottom and from the top of the upper beak was found. Our results also clearly show an effect of humidity on the stiffness of keratin, which is consistent with earlier reports [13].

5. CONCLUSION

Standard methods such as tensile tests and strain gauges are difficult to use on complex and small biological samples, such as the upper beak of small birds. Here, we present two alternative methods to obtain the Young modulus of such small samples. The double-indentation technique was used to obtain the modulus of thin pieces of keratin and bone. Second, an inverse analysis of a bending experiment, using measurement data from DSPI, was used for *in situ* material determination. Both methods were first tested on dry samples and provided consistent results. Young's moduli of 7.3 ± 0.6 and 3.1 ± 0.2 GPa were found for bone and dry keratin, respectively. Double-indentation testing was also used to obtain the modulus of fresh samples. No significant difference was found for bone, so the value for dry bone can be used. An effect of humidity on the elastic modulus of keratin was found and a modulus of 1.7 ± 0.4 GPa was obtained for fresh keratin.

Financial support for this project was given by the Research Foundation–Flanders (FWO). We thank F. Wiese and W. Deblauwe for their technical assistance and D. Adriaens and A. Genbrugge for their help with the interpretation of the beak histology and computed tomography scans.

REFERENCES

1 Richmond, B. G., Wright, B. W., Grosse, I., Dechow, P. C., Ross, C. F., Spencer, M. A. & Strait, D. S. 2005 Morphology, finite element analysis in functional. *Anat. Rec.* **283A**, 259–274. (doi:10.1002/ar.a.20169)

2 Ross, C. F. 2005 Finite element analysis in vertebrate biomechanics. *Anat. Rec.* **283A**, 253–258. (doi:10.1002/ar.a.20177)

3 Rayfield, E. J. Finite element analysis and understanding the biomechanics and evolution of living and fossil organisms. *Annu. Rev. Earth Planet. Sci.* **35**, 541–576. (doi:10.1146/annurev.earth.35.031306.140104)
4 Cobb, S. N. 2011 Craniofacial biomechanics: *in vivo* to *in silico*. *J. Anat.* **218**, 1–2. (doi:10.1111/j.1469-7580.2010.01328.x)
5 Strait, D. S., Wang, Q., Dechow, P. C., Ross, C. F., Richmond, B. G., Spencer, M. A. & Patel, B. A. 2005 Modeling elastic properties in finite-element analysis: How much precision is needed to produce an accurate model? *Anat. Rec. A Discov. Mol. Cell. Evol. Biol.* **283A**, 275–287. (doi:10.1002/ar.a.20172)
6 Rayfield, E. J. 2011 Strain in the ostrich mandible during simulated pecking and validation of specimen-specific finite element models. *J. Anat.* **218**, 47–58. (doi:10.1111/j.1469-7580.2010.01296.x)
7 Genbrugge, A., Herrel, A., Boone, M., Van Hooreneke, L., Podos, J., Dirckx, J., Aerts, P. & Dominique, A. In press. The head of the finch: the anatomy of the feeding system in two species of finches (*Geospiza fortis* and *Padda oryzivora*). *J. Anat.* (doi:10.1111/j.1469-7580.2011.01437.x)
8 Dumont, E. R. 2010 Bone density and the lightweight skeleton of birds. *Proc. R. Soc. B* **277**, 2193–2198. (doi:10.1098/rspb.2010.0117)
9 Soons, J., Herrel, A., Genbrugge, A., Aerts, P., Podos, J., Adriaens, D., de Witte, Y., Jacobs, P. & Dirckx, J. 2010 Mechanical stress, fracture risk and beak evolution in Darwin's ground finches (*Geospiza*). *Phil. Trans. R. Soc. B* **365**, 1093–1098. (doi:10.1098/rstb.2009.0280)
10 Boag, P. T. & Grant, P. R. 1981 Intense natural selection in a population of Darwin's finches (Geospizinae) in the Galapagos. *Science* **214**, 82–85. (doi:10.1126/science.214.4516.82)
11 Van Der Meij, M. A. A. & Bout, R. G. 2000 Seed selection in the Java sparrow (*Padda oryzivora*): preference and mechanical constraint. *Can. J. Zool.* **78**, 1668–1673. (doi:10.1139/z00-114)
12 Meyers, M., Chen, P., Lin, A. & Seki, Y. 2008 Biological materials: structure and mechanical properties. *Prog. Mater. Sci.* **53**, 1–206. (doi:10.1016/j.pmatsci.2007.05.002)
13 Taylor, A. M., Bonser, R. H. C. & Farrent, J. W. 2004 The influence of hydration on the tensile and compressive properties of avian keratinous tissues. *J. Mater. Sci.* **39**, 939–942. (doi:10.1023/B:JMSC.0000012925.92504.08)
14 Soons, J. A. M., Baere, I. & Dirckx, J. J. J. 2011 New double indentation technique for measurement of the elasticity modulus of thin objects. *Exp. Mech.* **51**, 85–95. (doi:10.1007/s11340-010-9340-8)
15 Soons, J. A. M., Aernouts, J. & Dirckx, J. J. J. 2010 Elasticity modulus of rabbit middle ear ossicles determined by a novel micro-indentation technique. *Hear. Res.* **263**, 33–37. (doi:10.1016/j.heares.2009.10.001)
16 Soons, J. & Dirckx, J. J. J. 2010 Full field displacement and strain measurement of small complex bony structures with digital speckle pattern interferometry and shearography. *Proc. SPIE Florianopolis* **7387**, 73870C. (doi:10.1117/12.870678)
17 Gröning, F., Liu, J., Fagan, M. J. & O'Higgins, P. 2009 Validating a voxel-based finite element model of a human mandible using digital speckle pattern interferometry. *J. Biomech.* **42**, 1224–1229. (doi:10.1016/j.jbiomech.2009.03.025)
18 Bright, J. & Gröning, F. 2011 Strain accommodation in the zygomatic arch of the pig: a validation study using digital speckle pattern interferometry and finite element analysis. *J. Morphol.* **272**, 1388–1398. (doi:10.1002/jmor.10991)
19 Panagiotopoulou, O., Curtis, N., O'Higgins, P. & Cobb, S. N. 2010 Modelling subcortical bone in finite element analyses: a validation and sensitivity study in the macaque mandible. *J. Biomech.* **43**, 1603–1611. (doi:10.1016/j.jbiomech.2009.12.027)
20 Panagiotopoulou, O., Kupczik, K. & Cobb, S. N. 2011 The mechanical function of the periodontal ligament in the macaque mandible: a validation and sensitivity study using finite element analysis. *J. Anat.* **218**, 75–86. (doi:10.1111/j.1469-7580.2010.01257.x)
21 Panagiotopoulou, O., Wilshin, S. D., Rayfield, E. J., Shefelbine, S. J. & Hutchinson, J. R. 2012 What makes an accurate and reliable subject-specific finite element model? A case study of an elephant femur. *J. R. Soc. Interface* **9**, 351–361. (doi:10.1098/rsif.2011.0323)
22 Sneddon, I. N. 1965 The relaxation between load and penetration in the axisymmetric Boussinesq problem for a punch of arbitrary profile. *Int. J. Eng. Sci.* **3**, 47–57. (doi:10.1016/0020-7225(65)90019-4)
23 Leendertz, J. & Butters, J. N. 1973 An image-shearing speckle-pattern interferometer for measuring bending moments. *J. Phys. E Sci. Instrum.* **6**, 1107–1110. (doi:10.1088/0022-3735/6/11/019)
24 Si, H. 2006 TetGen: a quality tetrahedral mesh generator and three-dimensional Delaunay triangulator. User's manual, version 1.4. See http://tetgen.berlios.de/.
25 Maas, S. & Weiss, J. A. 2008 FEBio: finite elements for biomechanics. User's manual, version 1.0. See http://mrl.sci.utah.edu/software/febio.
26 Franck, A., Cocquyt, G., Simoens, P. & De Belie, N. 2006 Biomechanical properties of bovine claw horn. *Biosyst. Eng.* **93**, 459–467. (doi:10.1016/j.biosystemseng.2006.01.007)
27 Wroe, S. 2008 Cranial mechanics compared in extinct marsupial and extant African lions using a finite element approach. *J. Zool.* **274**, 332–339. (doi:10.1111/j.1469-7998.2007.00389.x)
28 Aernouts, J., Couckuyt, I., Crombecq, K. & Dirckx, J. J. J. 2010 Elastic characterization of membranes with a complex shape using point indentation measurements and inverse modelling. *Int. J. Eng. Sci.* **48**, 599–611. (doi:10.1016/j.ijengsci.2010.02.001)
29 Evans, F. G. 1973 *Mechanical properties of bone*. Springfield, IL: Charles C. Thomas.